International Journal of the Physical Sciences Vol. 6(22), pp. 5171-5180, 2 October, 2011
Available online at http://www.academicjournals.org/IJPS
DOI: 10.5897/IJPS11.1072
ISSN 1992 - 1950 ©2011 Academic Journals

Full Length Research Paper

Design and modelling of a linear switched reluctance actuator for biomedical applications

MAHMOUD Imed[1]*, REHAOULIA Habib[1] and AYADI Mahfoudh[2]

[1]Unit Signal, Image and Intelligent Control of Industriel Systems (SICISI), University of Tunis, Tunisia.
[2]Laboratory of solid Mechanics, Structures and the Technological Development (LMSSDT), University of Tunis, Tunisia.

Accepted 18 August, 2011

This paper deals with a design of linear stepper motor for biomedical applications. The involved biomedical system is a syringe pump generally used for continuous drug infusion. The syringe pump consists of a linear switched reluctance motor (LSRM) coupled to a syringe plunger. In order to determine the axial force to control the syringe plunger, it was necessary to begin by evaluating the thrust force. The latter constituted the key element for designing the motor. Based on the concept of energy balance, a simplified analytical model was developed to predict the electromagnetic characteristics of the linear switched reluctance motor. The validity of results was ensured by direct comparison with the finite element method (FEM).

Key words: Linear switched reluctance motor, syringe pump, modelling, finite-element.

INTRODUCTION

Since the advent of pharmaceutical drugs, methods for administering the drugs have been sought. The infusion is a method of drug administration in continuous time and constant flow. Whatever the nature of the disease, infusion therapy is more effective when injected doses are balanced and evenly distributed in time. The fulfillment of these requirements could be achieved by the use of syringe pumps which technology is constantly evolving (Assan et al., 1981; Scherpereel, 1991; Kan et al., 2009).

Motorization of these biomedical systems is often ensured by a stepper rotating motor coupled via a reducer with a system of movement transformation (Boujemaa, 1994). The reduction and the transformation of movement are expensive, cumbersome and requiring a routine maintenance. In order to improve the system compactibility and to increase the accuracy of the mechanical transmission between the actuator and the plunger, this work is developed.

Admittedly, the linear actuator to be conceived must develop the axial effort necessary to control the syringe piston in the presence of the aqueous solution to perfuse. Indeed, the geometrical, mechanical, electric and electromagnetic dimensions depend on the axial effort to produce. Thus, it is necessary to begin by characterizing the thrust force to move the plunger. This is the object of the first part where the syringe is modelled. For that reason, an analytical approach is developed to evaluate the different forces and pressures involved. In addition, an experimental bench was conceived to determine the thrust force and validate the analytical model of the syringe.

Once the nominal thrust force is fixed, it serves to determine the geometric dimensions of the linear motor. These latter are obtained with the help of Maxwell-2D software (Uday, 2000; Ajengui, 2004; Hoadley, 2005).

The last stage consists of studying the motor thus designed and checking if it is able to develop the nominal force to move the syringe. Regarding the LSRM modelling, there are many approaches such as lookup-table techniques, magnetic equivalent - circuit analysis,

*Corresponding author. E-mail: imed_mahmoud@yahoo.fr. Tel: +00216 97129649.

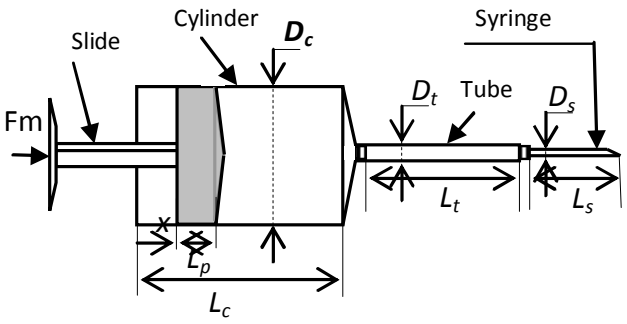

Figure 1. Schematic diagram of the syringe.

cubic-spline interpolations and finite-element analysis methods (FEM) (Kano et al., 2002; Xu et al., 2002; Srinivas et al., 2003; Chi, 2005; Ahmed, 2007).

To predict the motor electromagnetic characteristics, this paper presents an analytic representation of the winding linkage fluxes of the LSRM motor, as a function of position and current, taking into account the nonlinearity of the magnetic circuit. The variation of linkage fluxes with rotor position is expressed by a Fourier series in which the first three components are considered. Results of analytical approaches are compared with results which are those obtained by using finite-element methods.

SYRINGE MODELLING

The schematic diagram of the syringe, to be modelled, is illustrated by Figure 1 where all geometrical parameters are defined. We propose to study the driving force which is necessary to start and to maintain the movement of a plunger (or piston) inside a body of a medical infusion syringe.

Forces assessment

Total forces being exerted on the mover component are the driving action force F_m, the liquid action or compressive force F_p and the passive friction force F_r.

The compressive force is deduced from the pressure P applied to the plunger, it is expressed by relation (Equation 1) (Ellouze et al., 2010).

$$F_p = PS_c \quad (1)$$

With

$$S_c = \pi D_c^2 / 4 \quad (2)$$

where S_c is the cylinder section area of the syringe.

Two types of friction can occur on the contact cylinder-piston:

1. A sliding friction characterized by a coefficient f. Its intensity is proportional to the compression ratio of the elastic element ensuring the sealing:

$$F_g = fA(x)k(D_e - D_c) \quad (3)$$

where *A(x)* is the extent of contact slide/cylinder admitting for side surface $\pi D_c(L_p - x)$ with $0 < x < L_p$. This action is maximum for $x = 0$ and null for $x = L_p$.

2. A damping is caused by the presence of a liquid film which interposes interposed between the cylinder and the slide, when this one advances in the zone occupied initially by the liquid, of quantity x.

$$F_a = \eta x \frac{dx}{dt} \quad (4)$$

where $\eta = \rho v \pi D_c$ is the dynamic viscosity.

Pressure assessment

The infusion liquid is a real fluid of kinematic viscosity v, and density ρ will be supposed incompressible. With at balance, the total pressure P applied to the slide is equivalent to the infusion pressure P_p which is of the same order than the blood pressure. This one later is approximately 10 mm of mercury. In the event of infusion addition, the flow of the liquid generates pressure drop ΔP which come to be added to P_p. The pressure in the cylinder becomes (Murat, 2011; Kai et al., 2011):

$$P = Pp + \Delta P \quad (5)$$

These pressure drops ΔP includes the lineal pressure drop ΔP_l and the singular pressure drop ΔP_s. To ensure a stable infusion, it is necessary that the liquid flow in the various branches of the circuit (cylinder, syringe, tube) is carried out in laminar mode $R_e \prec 2000$, which is possible through a forward speed of the slide such that (Faisandier, 1999; Faroux et al., 1999):

$$\frac{dx}{dt} < \inf(2.10^3 \frac{\nu}{D}, \frac{L_d}{\tau}) \quad (6)$$

Where τ is the infusion estimated duration.

The different pressure drops are evaluated by the different lineal pressure drops in cylinder, tube and syringe are evaluated respectively by:

$$\Delta P_{lc} = 32\rho(L_d - x)\nu \frac{\dot{x}}{D_c^2} \quad (7)$$

$$\Delta P_{lt} = 32\rho L_t \nu D_c^2 \frac{\dot{x}}{D_t^4} \quad (8)$$

$$\Delta P_{ls} = 32\rho L_s \nu D_c^2 \frac{\dot{x}}{D_s^4} \quad (9)$$

Using Using Equations 7, 8 and 9, the resultant lineal pressure drop ΔP_l is obtained.

$$\Delta P_l = 32\rho\nu(L_d + L_t \frac{D_c^2}{D_t^4} + L_s \frac{D_c^2}{D_s^4})\frac{dx}{dt} - \frac{32\rho\nu}{D_c^2} x \frac{dx}{dt} \quad (10)$$

The singular pressure drop comes from the variations of the flow control sections. The Sections affected by these losses are connections cylinder-tube, tube- syringe and syringe-vein which will be taken for abrupt contracting of respective coefficient of constriction coefficient k_1, k_2 and k_3 (Faisandier, 1999; Faroux et al., 1999).

$$\Delta P_s = \frac{1}{2}(\frac{K_1}{D_t^2} + \frac{K_2}{D_s^2} + \frac{K_3}{D_v^2})\rho D_c^2 \left(\frac{dx}{dt}\right)^2 \quad (11)$$

Before the starting of the movement, it is necessary that the driving force can overcome the passive resistance F_g corresponding to $x = 0$. Notice that pressure drops are zero null in absence of flow. The initial driving force is then given by:

$$F_m = F_g(0) + PS = f\pi k L_p D_c (D_e - D_c) + \pi D_c^2 P_p / 4 \quad (12)$$

Once the movement is started and as long as the condition $x \prec L_p$ is checked, the movement of the slide obeys the differential equation:

$$F_m = m\frac{d^2x}{dt^2} + F_a + F_g + \pi(P_p + \Delta P_l + \Delta P_s)D_c^2/4 \quad (13)$$

The passive friction force defined as $F_r = F_m - F_g(0) - \pi D_c^2 P_p / 4$ can be presented in the form:

$$F_r = m\frac{d^2x}{dt^2} + C_1 x\frac{dx}{dt} + C_2\left(\frac{dx}{dt}\right)^2 + C_3\frac{dx}{dt} - C_4 x \quad (14)$$

For $x \succ L_p$ the sliding friction disappears ($F_g = 0$) and one will have:

$$F_r = m\frac{d^2x}{dt^2} + C_1 x\frac{dx}{dt} + C_2\left(\frac{dx}{dt}\right)^2 + C_3\frac{dx}{dt} = F_a \quad (15)$$

With

$C_1 = \eta - 8\pi\rho\nu$, $C_2 = \pi(\frac{K_1}{D_t^2} + \frac{K_2}{D_s^2} + \frac{K_3}{D_v^2})\rho D_c^4 / 8$

$C_3 = 8\rho\nu(L_d + L_t\frac{D_c^2}{D_t^4} + L_s\frac{D_c^2}{D_s^4})D_c^2$ and

$C_4 = f\pi D_c(D_e - D_c)$

SIMULATION AND EXPERIMENTAL VALIDATION

Solving Equations 14 and 15 for the geometrical quantities of a syringe of volume of 60 ml leads to the response of Figure 2, where a perfect linearity between the displacement of the syringe plunger x and the infusion time t is observed. Using this feature, we can record the values of theoretical time for the different volumes (60 ml, 30 ml, etc.) in order to compare it with time already determined from the experimental tests.

Actually, for the usual biomedical syringes, the thrust force which is necessary to overcome the plunger frictions is definitely higher than the effort of infusion. In order to quantify such friction, some tests were developed. An experimental bench was conceived according to Figures 3 and 4.

The body of the syringe is screwed onto a fixed support;

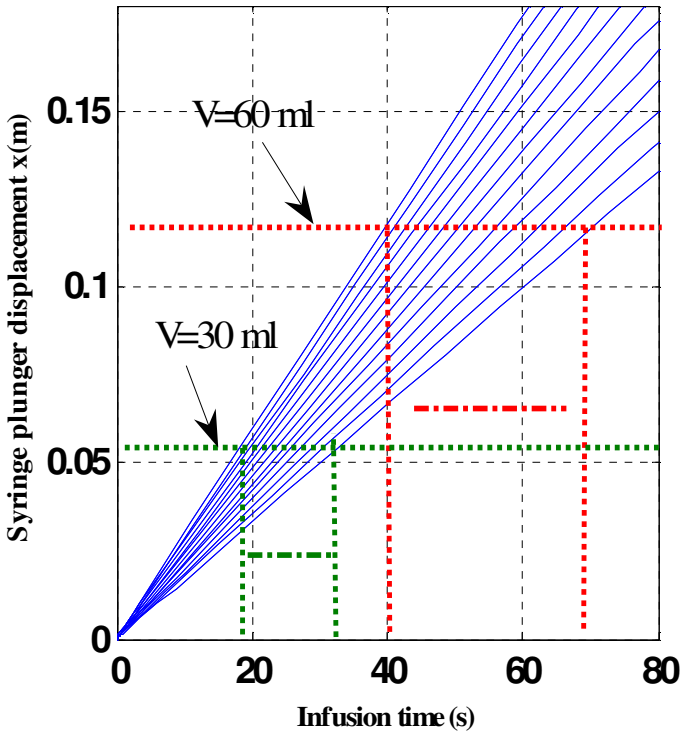

Figure 2. Theoretical characteristics of the syringe plunger displacement x versus infusion time t.

Figure 3. Experimental assembly for the determination of friction in the syringe.

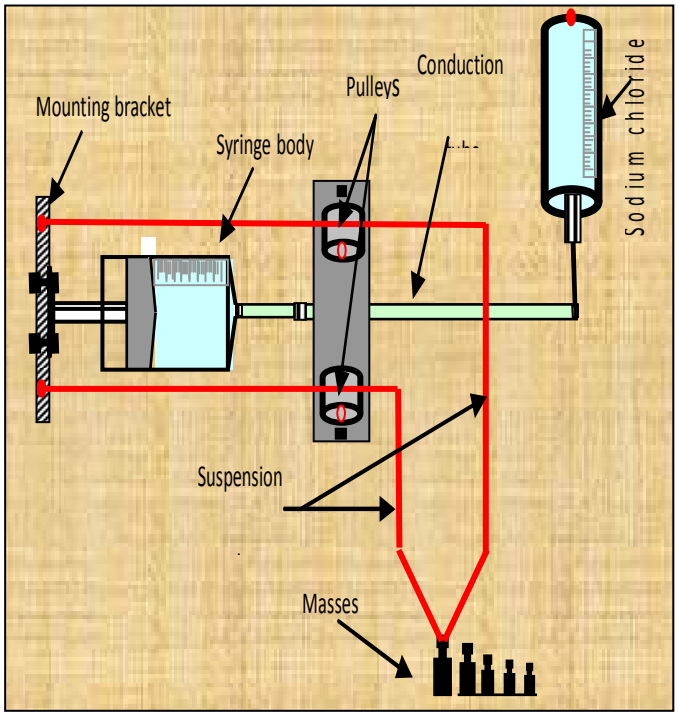

Figure 4. Schematic diagram of Figure 3.

the plunger is loaded to the marked masses suspended by two wires which are and balanced by two pulleys. Then, the weight is gradually increased until the piston begins to move. We proceed then, to note the corresponding infusion time for several piston positions at regular intervals. The enclosure containing the sodium chloride solution was introduced to simulate the patient blood pressure.

The evolution of the total efforts is reported in Figure 5. From Figures 2 and 5 were determined the theoretical and experimental values of time required for infusion.

In Figure 6, found points are all situated very close to first bisector, proving the almost equality between the experimental and theoretical times and the validity of the approach expressed by Equations 14 and 15.

Elsewhere, according to this study we deduce from Figure 5 that it is necessary for the incremental actuator to develop an axial thrust force of 4 N to move the piston. In what follows, it is reasonable to adopt a safety margin of 25% on the thrust force to avoid risks of malfunction.

DESIGN AND MAGNETIC CHARACTERISTICS OF THE LINEAR ACTUATOR

Linear motors with incremental movement can be made with various structures and varied principles. For reasons

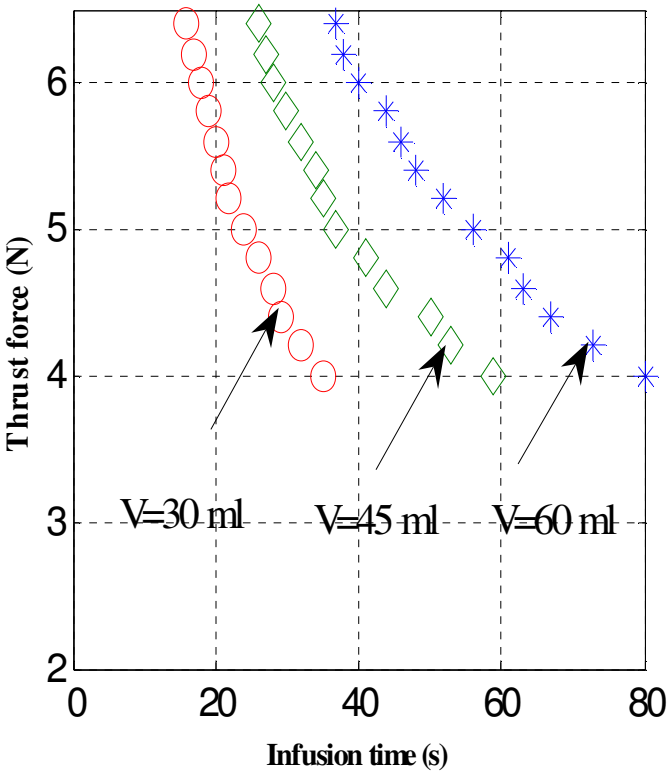

Figure 5. Experimental characteristics of the thrust force versus infusion time with sodium chloride solution for different volumes.

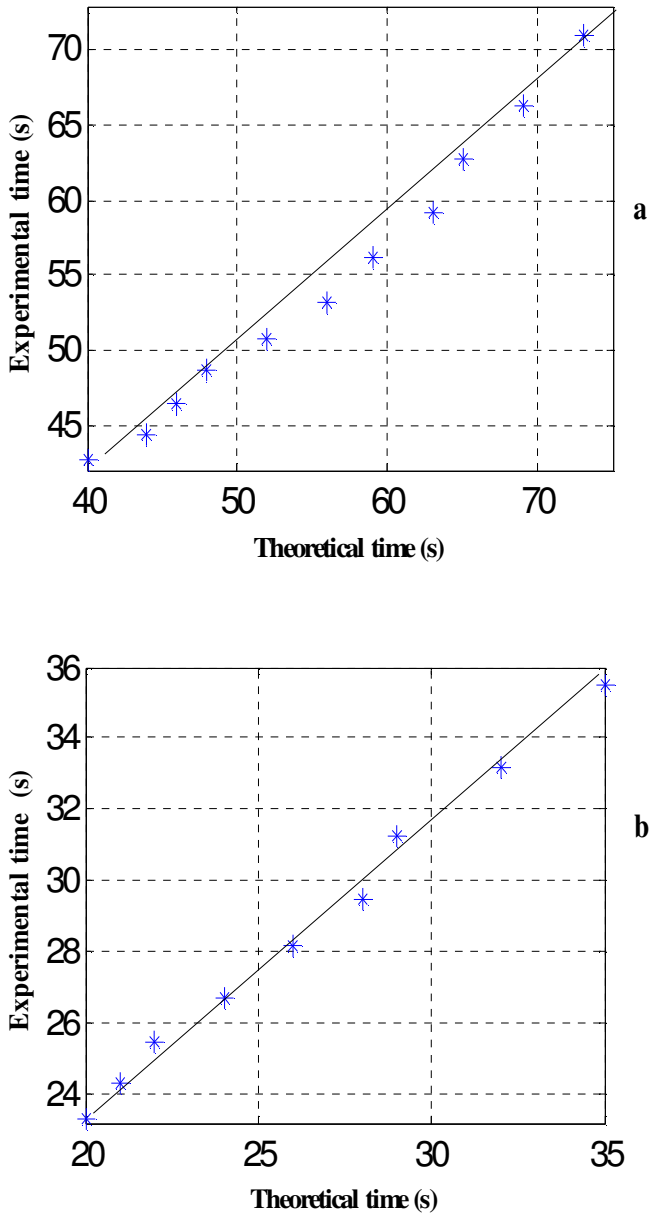

Figure 6. Experimental versus theoretical time required for infusion: (**a)** V=60 ml (full volume) and (**b)** V=30 ml (half volume).

of simplicity of construction and manufacturing cost, we opted for the plane linear structure with switched reluctance. This type of actuator is made up of a simply toothed sliding rail in translation on a whole of stator modules with plots regularly distributed (Figures 7 and 8). As the excitation is direct current (DC) and the translation is slow, the magnetic circuits can then be assembled using massive mild steel. The windings of the electric circuit are laminated with copper and they are concentrated around the cylinder heads of the stator. Non-magnetic separations are necessary between the various modules in order to impose a regular shift. Indeed, if teeth of active module are aligned with those of mover teeth, the other stator modules must be unaligned to create a translation force.

Taking into account geometrical dimensions of the syringe used in the operations of perfusion, a race of 96 mm segmented in steps of 1.5 mm seems to us an adequate choice for this actuator. On the basis of these two dimensions and by choosing a stator with four modules, it was possible to determine the geometrical parameters of the actuator. Some significant characteristics of the actuator are given in Table 1.

An understanding of the LSRM requires a detailed analysis of linkage fluxes and inductances for varying positions of the rotor and at different values of the stator excitation currents. The reluctance variation of the LSRM has an important role in the performance of this motor.

In order to characterize the magnetic behavior over the entire field of the machine under study, a computer program was developed around interpolation techniques. This program has allowed us to obtain databases illustrated in Figures 9, 10 and 11. These databases are

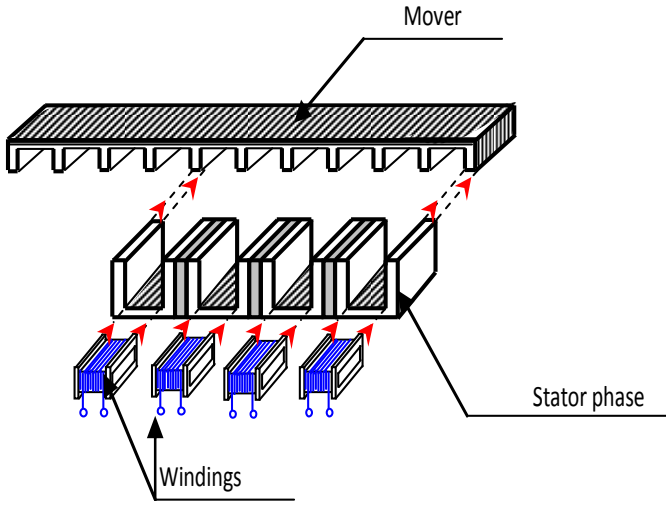

Figure 7. Structure of the linear actuator.

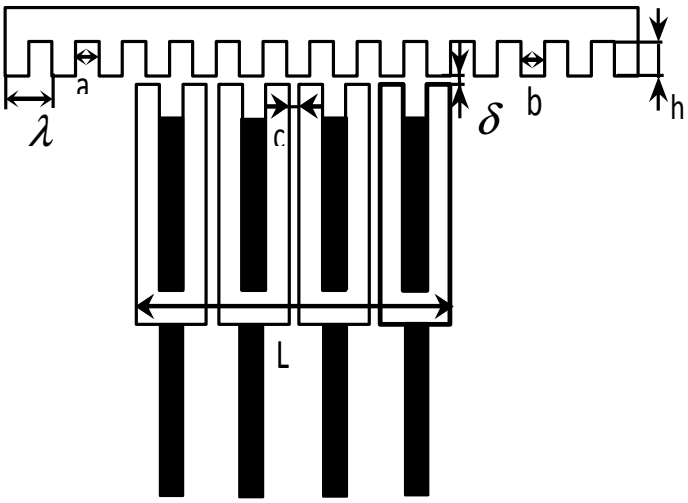

Figure 8. Main dimensions of the conceived actuator.

Table 1. Motor mechanical and electrical parameters.

Number of modules	4
Tooth width (b)	3 mm
Slot width (a)	3 mm
Tooth pitch (λ)	6 mm
Phase separation (c)	1.5 mm
Mover length	135 mm
Stator length (L)	40.5 mm
Air gap width (δ)	0.1 mm
Step size	1.5 mm
Number of turns per phase	520

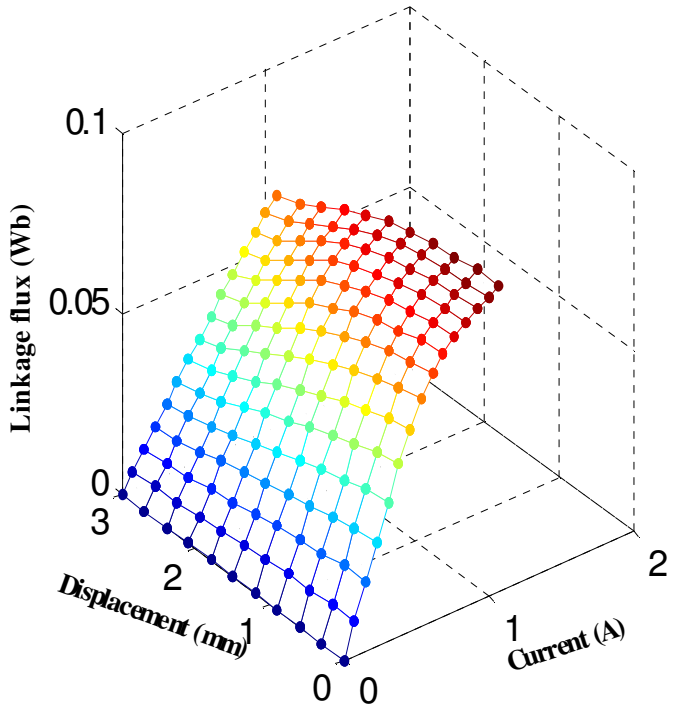

Figure 9. Linkage flux characteristics of a single winding with control current and different mover positions.

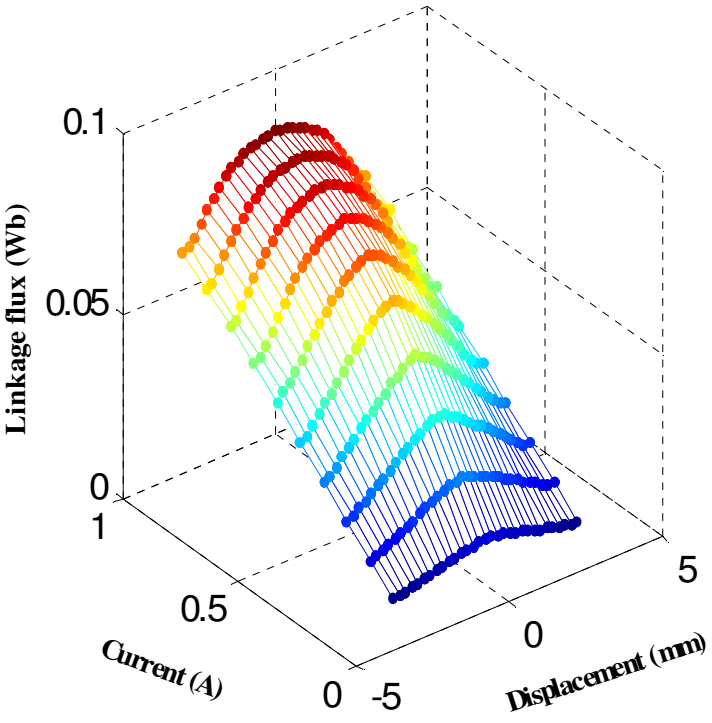

Figure 10. Response surface of the flux as a function of position and current.

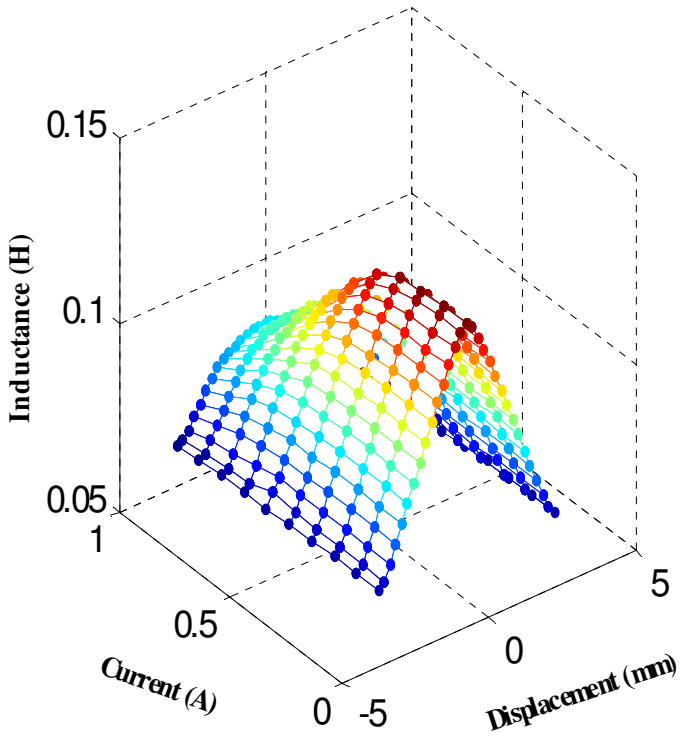

Figure 11. Response surface of the inductance as a function of position and current.

presented in the form of three-dimensional graphs, showing the characteristics of fluxes and the inductances (Jufer, 1995; Ahmed et al., 2000; Chevailler, 2006).

These results show that either linkage fluxes or self inductances are characterised by a maximum and a minimum. These two extreme values correspond in fact to the aligned and unaligned positions.

The extreme phases left and right of the actuator design conceived develop maximum thrust force of 10N, while intermediate stator modules generate a maximum force not exceeding 7 N (Figure 12). Clearly, for the same excitation current, the shape and the amplitude of the thrust force depend on the location of the coil excited in the stator stack. This asymmetry comes from the importance of magnetic leakages of central phases as compared to extreme phases. Moreover, the magnitude of this force also depends on the saturation level when the mobile moves.

The movement of the designed actuator conceived with four phases along a whole electric cycle is ensured by the juxtaposition of the thrust force developed successively by the four phases. For this type of actuator, the displacement is ensured by the thrust force defined by the intersections of its thrust force characteristics (Figure 12).

From this figure, the intersection between the angular characteristics of the various stator phases, guaranteed a thrust force of 5N which allows this actuator to control the considered biomedical system.

Analytical modelling of the LSRM

According to Ohm's and Faraday's laws, the applied voltage to a phase is equal to the sum of the resistive voltage drop and the rate of the linkages flux as:

$$u = Ri + \frac{d\varphi(i,x)}{dt} \tag{16}$$

R, i, φ are respectively resistance, current and linkage flux per phase whereas x designates the rotor position.

The force produced by an LSRM is proportional to the rate of change of co-energy as the rotor moves from one rotor position to another, as follows:

$$F(i,x) = \frac{\partial W_c(i,x)}{\partial x} \tag{17}$$

$$W_c(i,x) = \int_0^i \varphi(i,x)\,di \tag{18}$$

Using Equations 17 and 18, we get:

$$F(i,x) = \int_0^i \frac{\partial \varphi(i,x)}{\partial x} di \tag{19}$$

Finally, the mechanical equation evaluating the rotor acceleration, speed and position, as shown in Equation 20 (Nagel, 2000; Hur, 2003; Haijuin, 2009):

$$m\frac{dx^2}{dt^2} = F(x) - \xi\frac{dx}{dt} - F_0 signe\left(\frac{dx}{dt}\right) - F_c \tag{20}$$

Parameter m, ξ, F_0 and F_c designate the mover mass, the damp, the viscous friction force and the load force. They are supposed to be known for given motor and load. However, the action force F produced by a motor phase has to be evaluated for each mover position.

Since force F is estimated by Equation 19, analytical models differ simply by the different mathematical

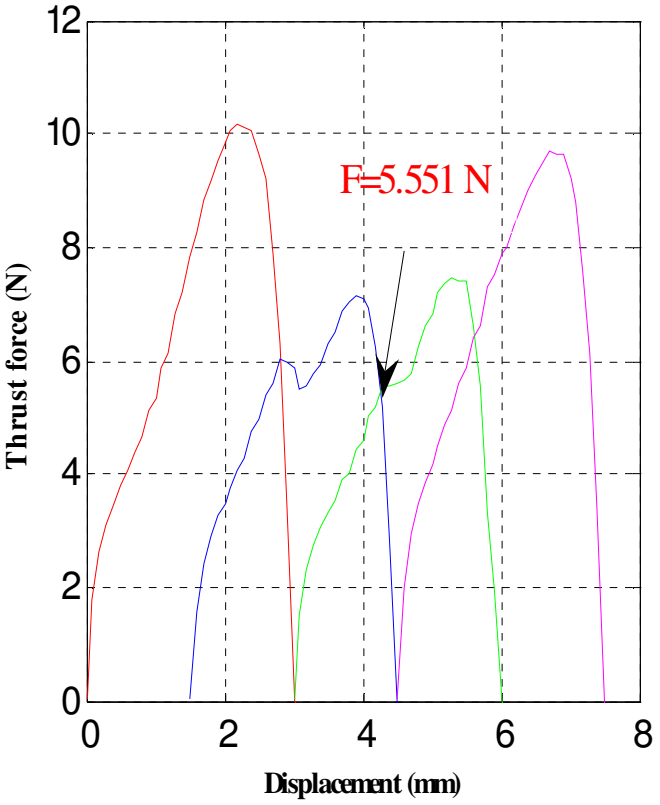

Figure 12. Characteristics of the thrust force for the four phases.

representations of the linkage flux.

The stator-phase linkage flux of the LSRM can be limited to the second harmonic order so that (Andrade, 2001; Ahmed, 2007; Adrian, 2009):

$$\varphi(i,x)=\varphi_0+\varphi_1\cos\left(\frac{2\pi}{\lambda}x\right)+\varphi_2\cos\left(\frac{4\pi}{\lambda}x\right) \quad (21)$$

For a given phase current, coefficients φ_0, φ_1 and φ_2 can be derived as functions of the aligned position linkage flux φ_c, the unaligned position linkage flux φ_{op} and the linkage flux at the midway φ_i, as follows:

$$\varphi_0=\frac{1}{2}\left[\frac{1}{2}\left(\varphi_c+\varphi_{op}\right)+\varphi_i\right] \quad (22)$$

$$\varphi_1=\frac{1}{2}\left(\varphi_c-\varphi_{op}\right) \quad (23)$$

$$\varphi_2=\frac{1}{2}\left[\frac{1}{2}\left(\varphi_c+\varphi_{op}\right)-\varphi_i\right] \quad (24)$$

Based on the earlier description, the proposed analytic modelling can be developed by using three curves: the aligned, the unaligned and the midway-position curves. Neglecting the effects of saturation and hysteresis, the unaligned position curve, as shown in Figure 13, is approximated by a straight line and can be described by:

$$\varphi_{op}=L_{op}i \quad (25)$$

where L_{op} is a constant that represents the equivalent inductance of the coil at the unaligned position.

Obviously, there is no linear relationship between linkage flux and current in the satured region for both aligned and midway positions. Multiplying linkage-flux (φ) by phase current (i) and plotting (φi) versus (i) (Figure 14), a linear relationship between (φi) and (i) can be observed in the satured region (Chi, 2005; Viorel, 2008; Padurariu, 2010). Consequently, the linkage flux of the aligned position shown in Figure 13 can be expressed as the linkage-flux of the aligned position shown in Figure 14 and can be expressed as:

$$\varphi_c=\begin{cases}L_c\,i & i\prec i_s\\ a_1-\dfrac{a_2}{i} & i\geq i_s\end{cases} \quad (26)$$

With

$$L_c\,i_s=a_1-\frac{a_2}{i_s} \quad (27)$$

In a similar way, the midway position can be expressed as:

$$\varphi_i=\begin{cases}L_i\,i & i\prec i_s\\ m_1-\dfrac{m_2}{i} & i\geq i_s\end{cases} \quad (28)$$

With

$$L_i\,i_s=m_1-\frac{m_2}{i_s} \quad (29)$$

where L_c and L_i are constants that represent the equivalent inductances of the coil, respectively in the aligned and midway positions in the unsaturated region.

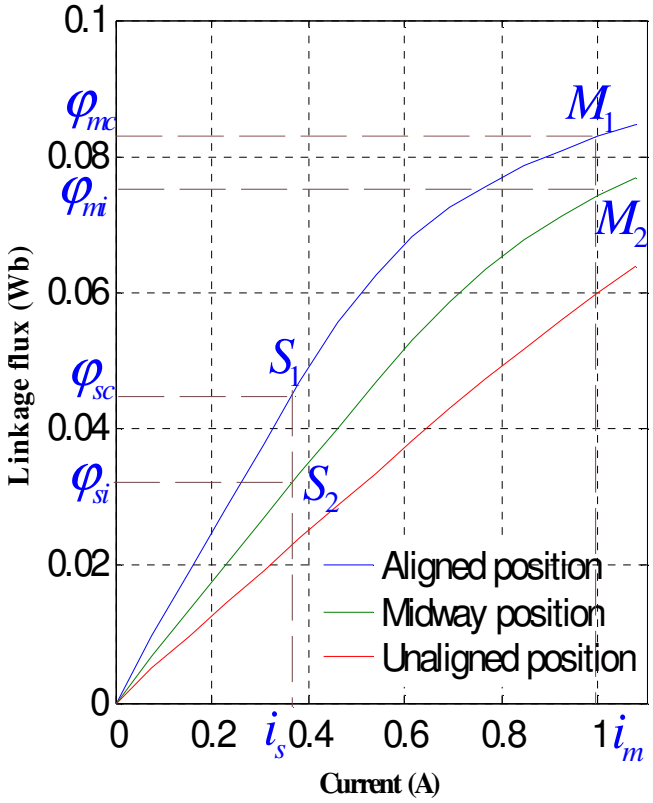

Figure 13. Linkage flux against phase current for different mover positions.

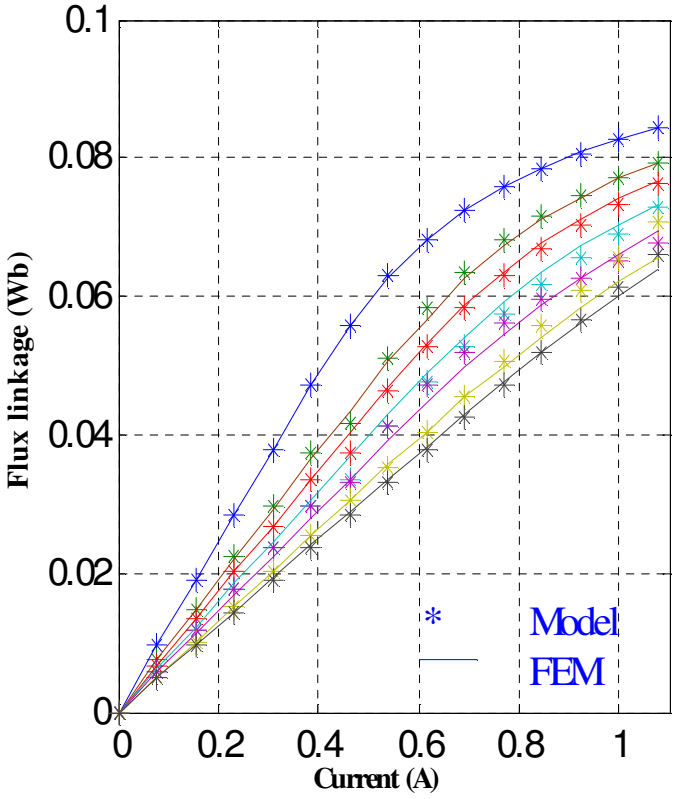

Figure 14. Extreme left phase: comparison of linkage flux versus current with different positions.

Constants a_1, a_2 and m_1, m_2 can be evaluated by using, respectively points (M_1, S_1) and (M_2, S_2) as shown in Figure 13.

Figure 14 gives the comparison of linkage flux produced by the left extreme phase versus current for different positions. It can be observed that the linkage-flux versus current for different position characteristics obtained by the proposed model closely match those obtained by finite element methods.

As shown previously, the electromagnetic force of the conceived motor is formulated by Equation 19. Now, the linkage flux is limited to the second order Fourier model as indicated by Equation 21 and its related relations of Equations 22, 23 and 24. After necessary mathematical manipulations, it is not difficult to get:

$$F = -\frac{1}{2}\left[\frac{2\pi}{\lambda}\sin\left(\frac{2\pi}{\lambda}x\right)\right]\left[\int_0^i \varphi_c di - \int_0^i \varphi_{op} di\right] - \left[\frac{2\pi}{\lambda}\sin\left(\frac{4\pi}{\lambda}x\right)\right]\left[\frac{1}{2}\int_0^i \varphi_c di + \frac{1}{2}\int_0^i \varphi_{op} di - \int_0^i \varphi_i di\right] \quad (30)$$

Electromagnetic force of Equation 30 is a highly nonlinear function with respect to the mover position and current. Figure 15 represents the comparison of the thrust force produced by the left extreme phase as function of mover position. Characteristics are calculated via proposed model and respectively by FEM (Padurariu, 2010). Evidently, the main difference comes from the choice of the mathematical model, specifically the linkage flux model (Equation 21). We expect that the accuracy may be improved by introducing higher order harmonics in Equation 21 and eventually by correctly choosing the number of Fourier terms.

CONCLUSION

This paper presents a study on a biomedical system formed by a syringe pump. First, an analytical model of the syringe plunger is developed followed by an experimental validation. Secondly, found results are exploited to design the LSRM used to move the plunger. Finally, a simple analytical model of the LSRM is presented in order to establish its electromagnetic characteristics.

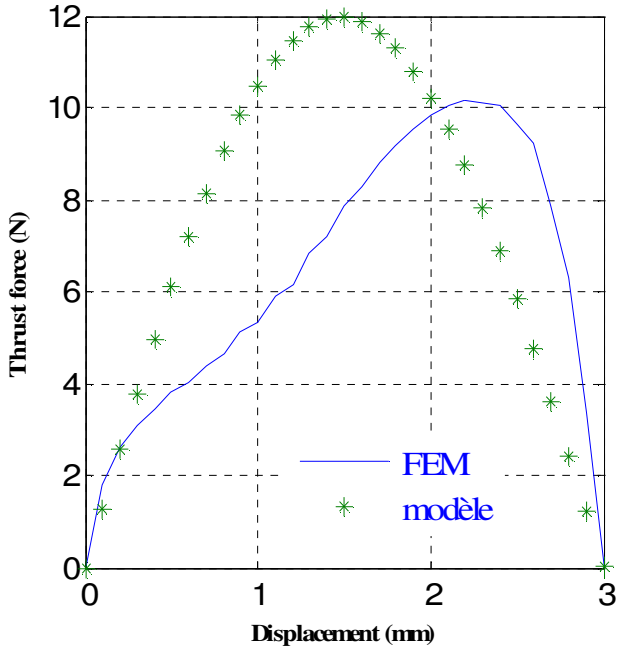

Figure 15. Extreme left phase: comparison of the thrust force as function of mover position.

Results are compared to those obtained via the 2D-FEM. The comparison shows a good reasonable agreement, proving the validity of the proposed approaches.

A work under study is undertaken to improve the accuracy of the analytical model by using higher order Fourier series.

REFERENCES

Adrian IV (2009). Analytical flux linkage model of switched reluctance motors. Rev. Roum. Sci. Techn. – Électrotechn. Énerg., 54(2):139–146.

Ahmed BH, Multon B, Prevond L, Lucidarme J (2000). Linear actuator integrated for automation application. Revue 3EI.

Ahmed K (2007). A Fourier Series Generalized Geometry-Based Analytical Model of Switched Reluctance Machines. IEEE transactions on industry application. 43(3).

Ajengui R (2004). Calculations approaches by finite elements of the thrust force of a tubular linear actuator. Automatic and signal treatment Master. National School Engineers of Tunis, Tunisia.

Andrade DA (2001). Characterization of Switched Reluctance Machines Using Fourier series Approach. Conference IEEE.

Assan R, Reach G, Poussier P (1981). Control glycemia and insulin treatment in surgical medium. Technicals manuals: pp. 728-729.

Boujemaa BS (1994). On the regulation of the syringes pump infusion controlled by stepper motor. International conference on electronic engineering. Oran: pp. 196-202.

Chevailler S (2006). Comparative study and selection criteria of linear motors. PHD no 3569, Ecole Polytechnique Fédérale de Lausanne à la faculté Sciences et Techniques de l'Ingénieur, Laboratoire d'actionneur intégrés.

Chi HP (2005). Simplified flux-linkage model for switched-reluctance motors. IEE Proc. Electr. Power Appl. 152(3).

Ellouze M (2010). Sliding mode control applied to a photovoltaic water pumping system. Int. J. Phys. Sci., 5(4): 334-344.

Faisandier J (1999). Hydraulic and pneumatic mechanisms. Dunod, Paris, ISBN :2-10-004074-X 8ème édition.

Faroux JP, Renault J (1999). Mechanics of the fluids and mechanical waves. Dunod, Paris, ISBN: 2-10-003434-0, 2ème années PC.

Haijuin Z (2009). Static characteristic and vibration dynamic reponse analysis of switched reluctance motor system. International conference on mechatronics and automation, proceeding of IEEE.

Hoadley R (2005). Basic User Manual Maxwell 2D Student Version.

Hur J (2003). Modelling of switched reluctance motor using Fourier series for performance analysis. J. Appl. Phys., 93(10).

Jufer M (1995). Electromechanics. Polytechnic presses and French Academics, Lausanne: 194-195.

Kai C, Hua Z (2011). An experimental study and model validation of pressure in liquid needle-free injection. Int. J. Phys. Sci., 6(7): 1552-1562.

Kan J, Tang K (2009). Study on a piezohydraulic pump for linear actuators. Sensors and Actuators. A 149: 331–339.

Kano Y, Kosaka T, Matsui N (2002). Magnetization characteristics analysis of SRM by simplified nonlinear magnetic analysis. Proc. Power Conversion Conf: pp. 689–694.

Murat K (2011). Vibration and stability of multi-cracked beams under compressive axial loading. Int. J. Phys. Sci., 6(11): 2681-2696.

Nagel NJ (2000). Modelling of a Saturated Switched Reluctance Motor Using an Operating Point Analysis and the Unsaturated Torque Equation. IEEE transactions on industry applications. 36(3).

Padurariu E (2010). Switched Reluctance Motor Analytical Models, Comparative Analysis. 12th International Conference on Optimization of Electrical and Electronic Equipment, OPTIM, IEEE.

Scherpereel P (1991). The diabetes is it a risk factor to the operation. National congress of Anaesthesia Reanimation, Ed. Masson. Paris: 31-40.

Srinivas KN, Arumugam R (2003). Dynamic characterization of switched reluctance motor by computer-aided design and electromagnetic transient simulation. IEEE Trans. Magn. 39(3):1806–1812.

Uday D (2000). Two-Dimensional Finite-Element Analysis of a High-Force-Density Linear Switched Reluctance Machine Including Three-Dimensional Effects. IEEE transactions on industry application. 36(4).

Viorel IA (2008). Speed-thrust Control of a Double Sided Linear Switched Reluctance Motor (DSL-SRM). Proceedings of the International Conference on Electrical Machines PaperID 879.

Xu Y, Torrey DA (2002). Study of the mutually coupled switched reluctance machine using the finite element-circuit coupled method. IEE Proc. Electr. Power. Appl., 149(2): 81–86.